Prediction of structural and metal-to-semiconductor phase transitions in nanoscale MoS2, WS2, and other transition metal dichalcogenide zigzag ribbons

F. Gueller, A. M. Llois, J. Goniakowski, Claudine Noguera

Prediction of structural and metal-to-semiconductor phase transitions in nanoscale MoS_2, WS_2, and other transition metal dichalcogenide zigzag ribbons

F. Güller,[1,2,3] A. M. Llois,[1,2,3,4] J. Goniakowski,[3,5,6] and C. Noguera[3,5,6]

[1]*Centro Atómico Constituyentes, GIyANN, CNEA, Av. Gral. Paz 1499, San Martín, Buenos Aires, Argentina*

[2]*Consejo Nacional de Investigaciones Científicas y Técnicas, Av. Rivadavia 1917 (C1033AAJ), Buenos Aires, Argentina*

[3]*Laboratorio Internacional Franco-Argentino en Nanociencias (LIFAN)*

[4]*Departamento de Física Juan José Giambiagi, FCEyN-UBA, Intendente Güiraldes 2160 (C1428EGA), Buenos Aires, Argentina*

[5]*CNRS, Institut des Nanosciences de Paris, UMR 7588, 4 place Jussieu, 75252 Paris cedex 05, France*

[6]*UPMC Université Paris 06, INSP, UMR 7588, 4 place Jussieu, 75252 Paris cedex 05, France*

(Received 24 October 2014; revised manuscript received 13 January 2015; published 5 February 2015)

While MoS_2 and WS_2 nanostructures gain an increasing importance in a number of recent technological applications, the control of their structure as a function of their size and their environment appears of prominent importance. In the present study which relies on first-principles simulations, we predict the dimerized 1T′ structural phase to be the actual ground state of MoS_2, WS_2, and $MoSe_2$ zigzag nanoribbons of small width and monolayer thickness. We assign this result to the competition between edge energy—which favors the nonpolar 1T′ edges over the polar 1H edges—and the energy of atoms in the center of the ribbons—which favors the 1H ground state of the infinite monolayers. A metal-to-semiconductor transition accompanies the structural transition. At variance, ZrS_2 zigzag ribbons are predicted to display the 1T structure whatever their width. In compounds of major technological importance, such structural and electronic flexibility associated with polarity effects opens the possibility for controlling the ribbon type during synthesis.

DOI: 10.1103/PhysRevB.91.075407 PACS number(s): 61.46.−w, 73.22.−f, 73.90.+f, 77.22.Ej

I. INTRODUCTION

Similarly to graphene, atomically thin films of inorganic compounds such as hexagonal boron nitride, transition metal dichalcogenides (TMD), or oxides represent a promising family of materials for innovative applications, due to their electronic, optical, catalytic, and mechanical properties [1,2]. They can now be prepared by several methods, including ionic species intercalation, mechanical or liquid exfoliation, or by all traditional methods of deposition on a substrate. Nanostructures formed out of them, such as two-dimensional (2D) islands or nanoribbons, have also received much attention. More specifically, for TMD, there have been reports of unusual edge states in triangular MoS_2 [3–6] and WS_2 [7] islands, and theoretical evidences of metallicity and magnetism at nanoribbon zigzag edges of MoS_2 [6,8–12] or WS_2 [13,14]. The role of polarity on the electronic structure of such objects has recently been highlighted [15].

The properties of low dimensional nano-objects are strongly dependent upon their thickness/width, their stoichiometry, and their environment. It is, for example, well known that, below the so-called scalable regime, cluster structures may be totally different from the bulk one due to the increased energy weight of low coordinated atoms (e.g., surface versus bulk atoms). The same is true in ultrathin films or 2D nano-objects, especially when polarity effects are involved [16,17]. For example, to avoid the energy cost of surface polarity, at ultralow thickness, films of MgO(111) [18] or ZnO(0001) [19–22] have been predicted and found to display a stacking of flat/distorted graphenelike monolayers, as found in the hexagonal BN structure, rather than the expected rocksalt or wurtzite structure. TMD ultrathin films also display some structural flexibility. For example, in the single layer MoS_2 ground state, here labeled 1H, each Mo has a trigonal prismatic coordination with the nearby S atoms. However, it displays a 1H/1T phase transition, associated with a semiconducting to metal change of the electronic properties at high temperature [23] or when monolayers are exfoliated by Li intercalation [24–28]. At variance to the 1H polytype, in the 1T phase, each Mo is octahedrally coordinated with the nearby S atoms. Two recent theoretical studies of the metastable 1T phase in single layer MoS_2 have shown that it is actually unstable with respect to dimerization, giving way to a so-called 1T′ phase, which, however, remains less stable than the 1H phase [29,30]. Figure 1 shows the atomic arrangements in these three phases.

Here, going down in dimensionality and relying on first-principles simulations, we demonstrate that, in MoS_2, WS_2, and $MoSe_2$ monolayer-thick nanoribbons with zigzag edges, the 1T′ phase is the actual (low temperature) ground state when the ribbon width is small. Above a critical width, a transition towards the expected 1H phase takes place, accompanied by a metal to semiconducting transition in the electronic properties. We assign this ground state modification at small width to the general effect of edge polarity. The same argument explains why there is no similar transition for ZrS_2 whose infinite monolayer ground state is 1T, and why it is unlikely to occur in (nonpolar) armchair nanoribbons.

The paper is organized as follows. After a brief description of the method used (Sec. II) and its application to infinite monolayers (Sec. III), we present the structural phase diagram as a function of thickness for the four compounds (Sec. IV). Then we analyze the mechanism of stabilization of the small width structure (Sec. V), before concluding (Sec. VI).

II. SIMULATION SETUPS

All calculations are performed using *ab initio* spin polarized density functional theory as implemented in VASP [31]. PAW pseudopotentials are used [32], together with the generalized gradient approximation as parametrized by Perdew *et al.* [33]

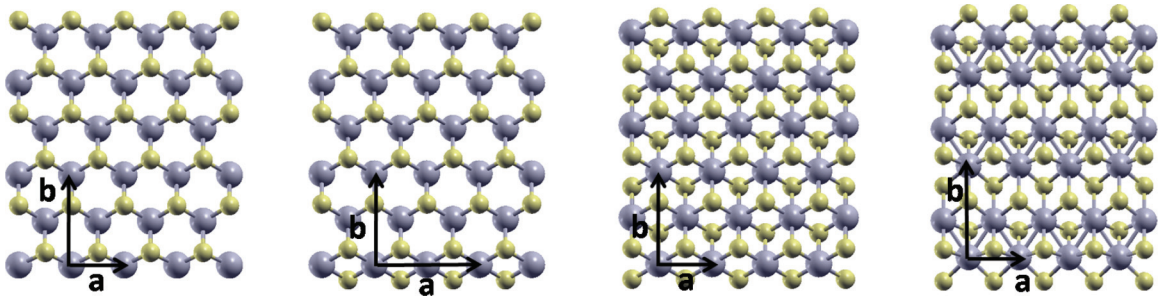

FIG. 1. (Color online) From left to right, top view of 1H, 1H*, 1T, and 1T′ MoS_2 monolayers/ribbons: Mo (gray) and S (yellow). Rectangular unit cell vectors are explicitly plotted. If the structures shown are considered periodic only in the a direction, they correspond to the $N = 6$ zigzag nanoribbons. In the 1H* ribbons, the unit cell vector a is doubled due to a different relaxation of neighboring edge atoms.

for the exchange and correlation potential. Self-consistent iterations are carried out until the difference in total energy between successive steps is smaller than 10^{-6} eV. The kinetic energy cutoff for the plane waves is set equal to 225 eV and all structures are fully relaxed until residual forces drop below 0.01 eV/Å.

Infinite monolayers are separated by a vacuum region of at least 10 Å. A fine $(17 \times 17 \times 1)$ Monkhorst-Pack k-point grid is used for the undistorted 1H and 1T (1×1) unit cells. To account for a possible dimerization, 1T′ calculations are performed in a rectangular cell [$(17 \times 10 \times 1)$ k-point sampling] with a full optimization of both lattice parameters a and b.

The unit cells used for ribbon simulations have 16 Å in the direction perpendicular to the ribbon plane, and 35 Å in the in-plane direction perpendicular to the edges. Ribbons of width N and unreconstructed edges involve $3N$ atoms in their unit cell, whether in the 1H, 1T, or 1T′ phase. For these systems, the k-point grid in the first Brillouin zone of the nonreconstructed ribbon is $(17 \times 1 \times 1)$. Charges are calculated according to Bader's prescription [34,35].

III. INFINITE MONOLAYERS

Our study focuses on four semiconducting compounds: MoS_2, WS_2, $MoSe_2$, and ZrS_2. These TMDs have layered structures consisting of a stacking of 2D monolayers, mainly held together through weak van der Waals interactions. Each monolayer is composed of a plane of transition metal atoms (Mo, W, or Zr) sandwiched by two planes of chalcogen atoms (S, Se). The strong bonding between metal and chalcogen atoms within the monolayer has a mixed ionic and covalent character. Several monolayer polytypes exist, 1H when metal atoms have trigonal prismatic coordination, 1T when they are in octahedral coordination, and 1T′ resulting from the dimerization of 1T (Fig. 1). MoS_2, WS_2, $MoSe_2$, and ZrS_2 present different bulk stackings and different degrees of covalency in the metal-chalcogen bonding.

We have simulated infinite 1H, 1T, and 1T′ monolayers for the four compounds. Their structural, electronic, and energetic characteristics are summarized in Table I. For the sake of a better comparison, they are all described within a rectangular unit cell containing two formula units. As expected from their bulk structure, we find that the hexagonal 1H configuration is the most stable for the MoS_2, WS_2, and $MoSe_2$ monolayers. We agree with previous studies about the stabilization of the MoS_2 1T′ structure by dimerization, and we predict that a similar distortion also happens in $MoSe_2$ and WS_2 1T states. The dimerization leads to substantial energy lowering with respect to the 1T state (0.29, 0.33, and 0.33 eV per formula unit, for MoS_2, WS_2, and $MoSe_2$, respectively). In ZrS_2, the energy difference between the two phases is at the limit of precision of our simulation.

As far as electronic properties are concerned, due to Zr low electronegativity, ZrS_2 is the most ionic of the four compounds, with cationic charges 2–4 times larger than in other TMDs according to Bader's charge decomposition. Its three structural phases are semiconducting (HOMO-LUMO gap equal to 0.85, 1.2, and 1.1 eV in 1H, 1T, and 1T′, respectively). At variance, MoS_2, WS_2, and $MoSe_2$ are semiconducting in their 1H phase (HOMO-LUMO GGA gaps equal to 1.56, 1.90, and 1.51 eV, respectively) but metallic in the 1T phase. Dimerization either preserves their metallic character or opens a tiny gap [30]. As expected, MoS_2 turns out to be more ionic, with a larger

TABLE I. Structural and electronic characteristics of infinite 1H, 1T, and 1T′ monolayers: lattice parameters a and b of a rectangular unit cell ($b = a\sqrt{3}$ for 1H and 1T), nearest-neighbor metal-S/Se distances d (Å), cationic charges Q (e), difference of formation energies E_{form} (eV/formula unit) with respect to the most stable structure, and HOMO-LUMO band gap (eV).

	a (Å)	b (Å)	d (Å)	Q (e)	E_{form} eV/f.u.	Gap (eV)
MoS_2						
1H	3.19	5.52	2.41	+1.18	0.00	1.56
1T	3.19	5.54	2.43	+1.21	0.83	0.00
1T′	3.21	5.71	2.40–2.54	+1.18/+1.25	0.54	0.00
WS_2						
1H	3.20	5.54	2.43	+0.95	0.00	1.90
1T	3.22	5.58	2.44	+0.90	0.88	0.00
1T′	3.20	5.76	2.43–2.57	+1.31–1.26	0.55	0.04
$MoSe_2$						
1H	3.32	5.75	2.55	+0.47	0.00	1.51
1T	3.29	5.70	2.57	+0.50	0.70	0.00
1T′	3.26	6.04	2.53–2.70	+0.49/+0.56	0.37	0.00
ZrS_2						
1H	3.57	6.19	2.59	+2.07	0.56	0.85
1T	3.69	6.38	2.57	+2.06	0.00	1.2
1T'	3.68	6.39	2.57–2.58	+2.06/+2.05	0.00	1.1

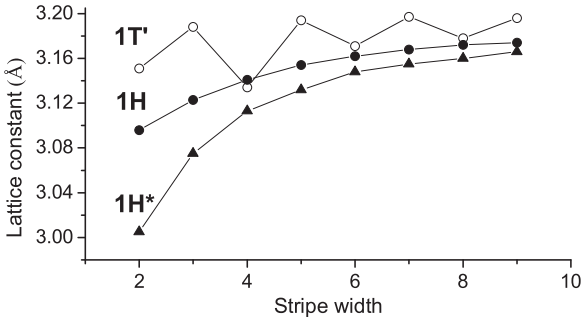

FIG. 2. Optimized lattice constants of WS_2 polar 1H (filled circles), $1H^*$ (filled triangles), and nonpolar $1T'$ (open circles) zigzag ribbons.

electron transfer from the chalcogen towards the TM atom, than WS_2 and, to a larger extent, than $MoSe_2$.

To conclude on infinite monolayers, the characteristic, which will turn out to be the most relevant in the following, is the rather low energy difference between 1H and $1T'$ structures. This opens the possibility of stability reversals in low dimensional objects formed from these monolayers, due to edge effects.

IV. ENERGETICS OF ZIGZAG NANORIBBONS

Stoichiometric zigzag nanoribbons of increasing width, formed out of 1H, 1T, and $1T'$ monolayers of each compound, have been simulated, as shown in Fig. 1. Cuts of a 1H monolayer produce ribbons (labeled 1H) with a cationic termination on one side and an anionic one on the other. This asymmetry results from the absence of inversion symmetry center in the structure. A more stable stoichiometric configuration (labeled $1H^*$) may be obtained if edge cations are bridged by S/Se atoms and half of the S/Se atoms are removed from the anionic edge (with a doubling of the unit cell in the a direction), as proposed in Ref. [9]. As regards 1T and $1T'$ ribbons, it is possible to generate structures with chalcogen atoms on both borders. The doubling of the unit cell in the b direction produces odd-even oscillations of the lateral lattice constant a as a function of thickness as shown in Fig. 2, which are not present in the 1H ribbons. In all cases, a converges asymptotically to a constant value corresponding to that of the infinite monolayers.

Since all atoms count in a nano-object, the relative stability of the 1H, $1H^*$, 1T, and $1T'$ zigzag nanoribbons may be assessed by their formation energy per unit edge length, referred to the monolayer ground state energy:

$$E_{\text{form}}(N) = \frac{E_{\text{tot}}(N) - NE_{\infty}}{a}. \quad (1)$$

In this expression, $E_{\text{tot}}(N)$ is the total energy of a ribbon containing N formula units in the periodic cell, E_{∞} is the energy per formula unit in the infinite monolayer ground state (1H for MoS_2, WS_2, and $MoSe_2$, 1T for ZrS_2), and a is the optimized ribbon lattice parameter.

The ribbon formation energy $E_{\text{form}}(N)$ includes the edge and electrostatic contributions, which tend to constant values at large widths, and an additional one if the ribbon does not adopt the ground state structure of the infinite monolayer. This is the case for $1T'$ ribbons of MoS_2, WS_2, and $MoSe_2$, and for

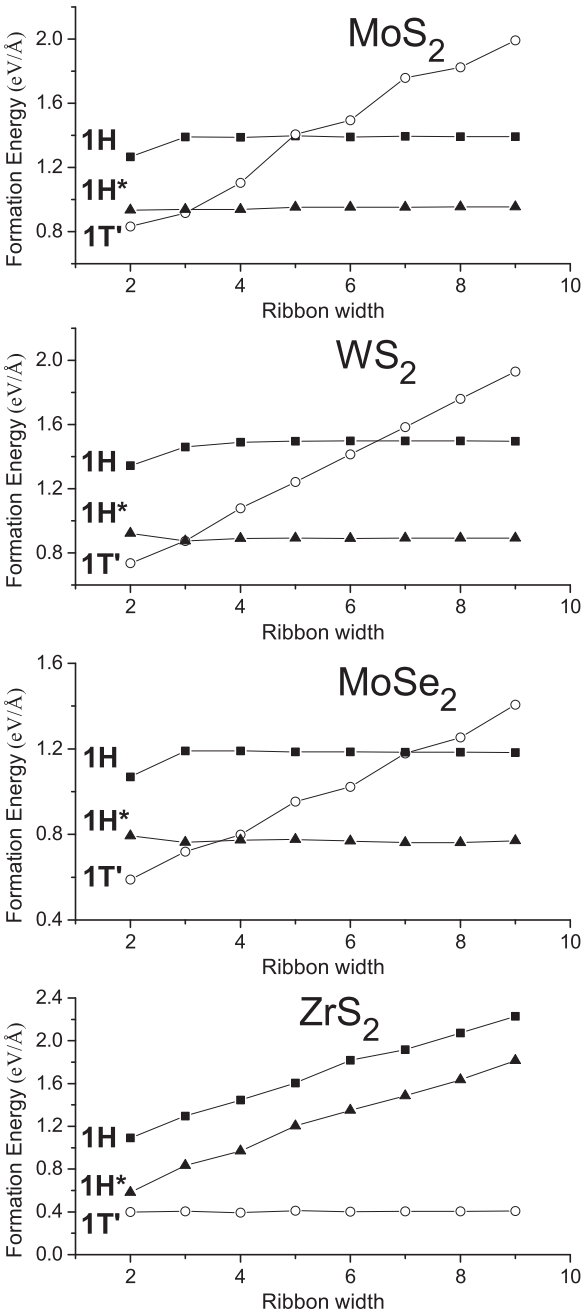

FIG. 3. From top to bottom, formation energies per unit length of MoS_2, WS_2, $MoSe_2$, and ZrS_2 1H (filled squares), $1H^*$ (filled triangles) and $1T'$ (open circles) ribbons, as a function of ribbon width.

$1H/1H^*$ ribbons of ZrS_2. This additional contribution grows linearly with the ribbon width, with a slope proportional to $E_{\infty}^{1T'} - E_{\infty}^{1H}$ in the first case and $E_{\infty}^{1H} - E_{\infty}^{1T'}$ in the second.

As shown in Fig. 3, aside from small odd-even oscillations displayed by the $1T'$ formation energy curves, which are associated with the dimerization and also show up in the lattice parameter curve (Fig. 2), the most striking result evidenced in Fig. 3 is the existence of a stability inversion between the $1T'$ and $1H/1H^*$ phases, in MoS_2, WS_2, and $MoSe_2$ ribbons as a function of width. Our simulations predict that narrow zigzag ribbons of these compounds have a dimerized $1T'$

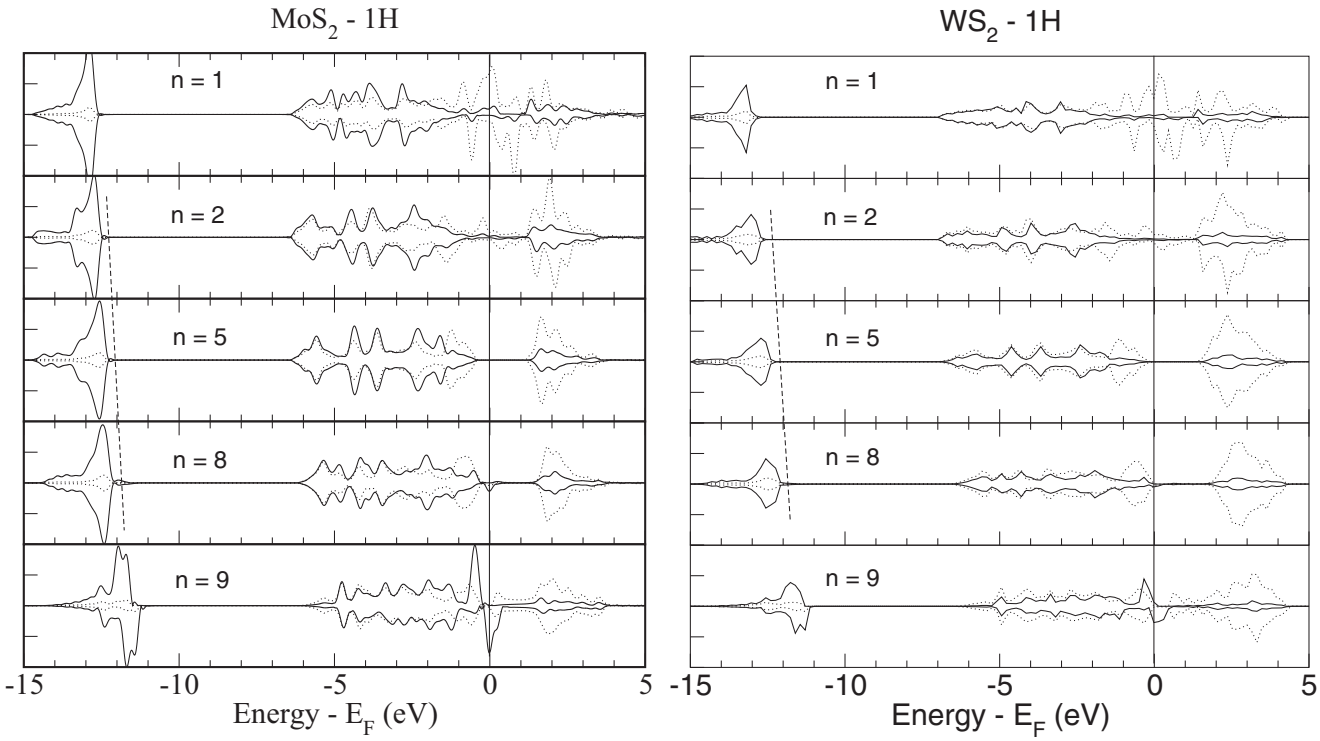

FIG. 4. Row-projected densities of states across 1H $N = 9$ nanoribbons. Left: MoS_2, right: WS_2. Rows 3 and 4 and 6 and 7 are skipped for simplicity. The Fermi level is at zero energy. Solid (dotted) lines correspond to S (Mo/W) projections. The dashed line is a guide for the eyes and shows the shift of the semicore S states across the ribbon.

ground state structure, which only gives way to the 1H/1H* phase characteristic of the infinite monolayer, above a critical width. This critical width is equal to $N_c = 3$ for the $1T' - 1H^*$ transition for the three compounds and $N_c = 5$, 6, and 7, for the 1T′-1H transition in MoS_2, WS_2, and $MoSe_2$ ribbons, respectively. In the following section we present arguments for assigning the stabilization of 1T′ phase to edge polarity effects.

V. MECHANISM OF STABILIZATION OF THE 1T′ PHASE OF MoS_2, WS_2, AND $MoSe_2$

The row-projected local densities of states (DOS) and the Bader charges across $N = 9$ MoS_2 and WS_2 zigzag ribbons in the 1H, 1H*, and 1T′ structures are shown in Figs. 4–7. The characteristics of 1H/1H* ribbons bear strong resemblances with polarity characteristics in thin films [16,17]. Indeed, the repeat unit in the *b* direction bears a dipole moment, resulting from the alternation of positively charged TM and negatively charged chalcogen rows. The electrostatic potential associated with the total dipole shifts the projected densities of states on successive rows—particularly visible on the semicore states—and induces an overlap of the valence and conduction bands on opposite edges of the ribbon. This overlap and the resulting partial filling of edge bands provide the compensating charges necessary for polarity healing. Due to the polar character of their edges, zigzag nanoribbons of 1H/1H* structure have a quite large formation energy.

Polarity compensation effects in the 1H* ribbons are however weaker than in the 1H ribbons, explaining a part of their energy difference. Indeed, due to the 1/3 ratio between successive inter-row distances, a compensating surface charge density $\delta\lambda$ equal to $\pm\lambda/3$ is required to cancel the monolayer polarization (λ is the charge density of atomic rows in the center of the ribbon) [17]. The Bader charges (Fig. 7) and row-projected DOS (Figs. 4–6) show that, in the 1H case, a shift of the DOS structure across the ribbon results in an overlap of edge states of the opposite ribbon edges and in an electron transfer from anionic to cationic edge which produces the required $\delta\lambda = \lambda/3$. In the case of 1H* ribbons, the additional S/Se atoms on the cationic edge and the missing S/Se atoms on the anionic edge provide additional edge charges equal to $\mp\lambda/2$. The electron transfer between ribbon edges necessary to heal the polarity is thus smaller and equal to $\mp\lambda/6$ only. This value, being lower than the 1H one, has a lower energy cost. Added to the fact that 1H* edge cations have a more favorable sixfold coordination, this results in a lower formation energy of 1H* ribbons compared to their 1H counterparts. We note that, in agreement with these arguments, compensating edge charge densities of electronic origin have opposite signs in 1H and 1H* ribbons [Fig. 7] and are associated with opposite shifts of the DOS structures across the two types of ribbons [Figs. 4 and 5].

On the other hand, 1T and 1T′ zigzag ribbons are nonpolar. This is not because they bear no *total* dipole moment. As discussed elsewhere [17], the actual reason stems from the absence of dipole moment in the repeat unit perpendicular to the edges (Fig. 1). The row-projected local DOS and the Bader charges across $N = 9$ 1T′ ribbons, in MoS_2 and WS_2, displayed in Figs. 6 and 7, clearly demonstrate that there is no band shift across the ribbons nor compensating charges in the 1T′ ribbons. Absence of band gap in

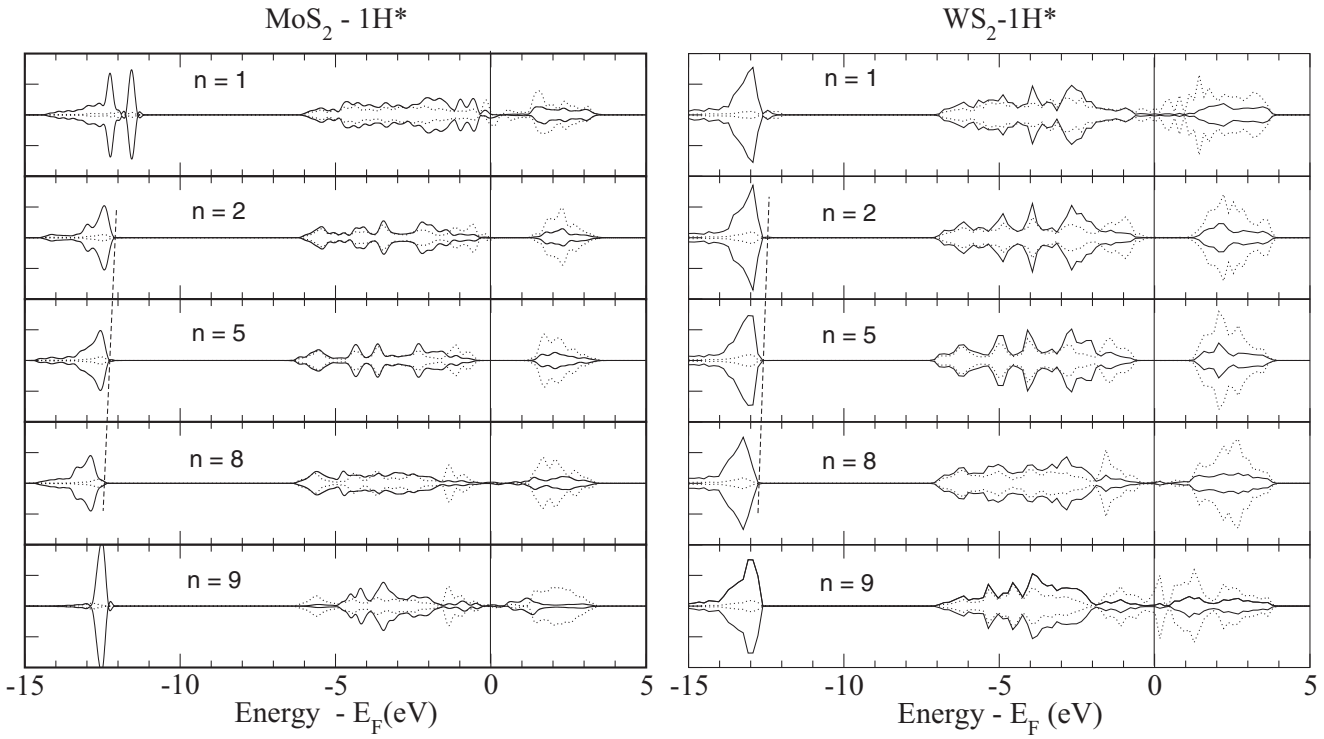

FIG. 5. Row-projected densities of states across 1H* $N = 9$ nanoribbons. Left: MoS_2, right: WS_2. Rows 3 and 4 and 6 and 7 are skipped for simplicity. The Fermi level is at zero energy. Solid (dotted) lines correspond to S (Mo/W) projections. The dashed line is a guide for the eyes and shows the shift of the semicore S states across the ribbon.

the center of the ribbon is a characteristic of the infinite 1T′ monolayers. Similar results are found for $MoSe_2$ and ZrS_2.

In narrow ribbons, due to the important ratio of edge-to-"bulk" atoms (bulk atoms here meaning atoms in the center of the ribbon), the edge energy terms may become competitive or

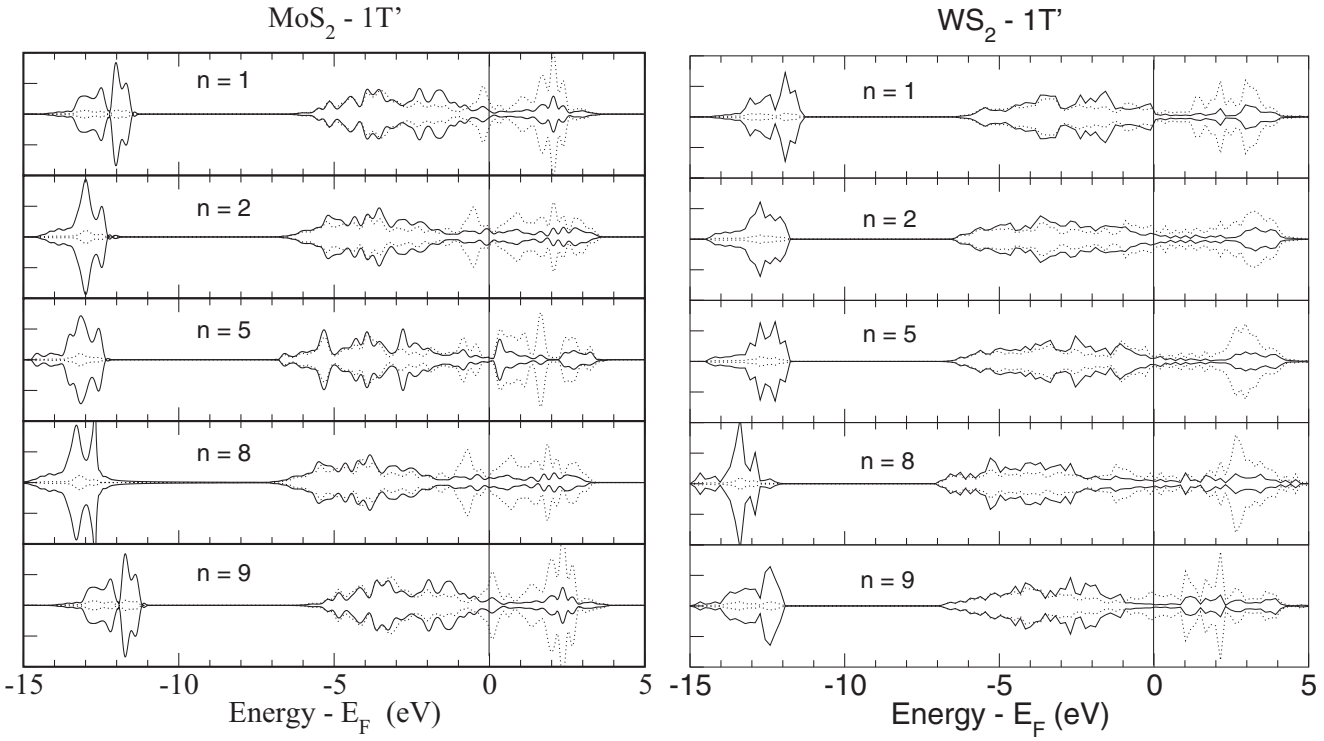

FIG. 6. Row-projected densities of states across 1T′ $N = 9$ nanoribbons. Left: MoS_2, right: WS_2. Rows 3 and 4 and 6 and 7 are skipped for simplicity. The Fermi level is at zero energy. Solid (dotted) lines correspond to S (Mo/W) projections.

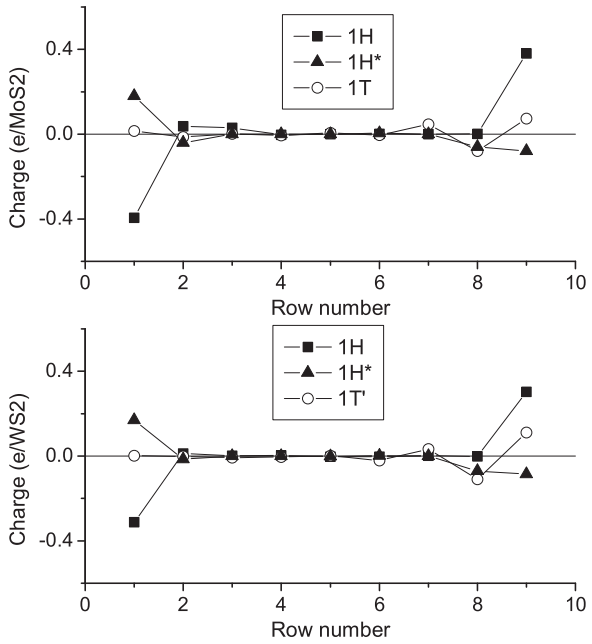

FIG. 7. Values of row projected Bader charge modifications with respect to central row of the $N = 9$ nanoribbons. Top: MoS_2; bottom: WS_2.

even overcome the bulk ones. In MoS_2, WS_2, and $MoSe_2$, bulk atoms are better stabilized in the 1H configuration which is the ground state of the infinite monolayers, while 1T′ configuration is more favorable to edge atoms due to the nonpolar character of the edges. As a consequence, since nonpolar edges are generally more stable than polar ones, the 1T′ phase turns out to be the ground state for narrow zigzag ribbons. But this is only possible up to a critical width N_c, since each additional row in the 1T′ structure costs the $E_\infty^{1H} - E_\infty^{1T'}$ energy difference.

This mechanism explains the stabilization of the 1T′ ribbon phase in MoS_2, WS_2, and $MoSe_2$ narrow ribbons. It is further confirmed by the absence of stability inversion in ZrS_2 ribbons. Since the 1T′ configuration is the ground state of the infinite monolayer, and its zigzag edges are nonpolar, bulk and edge energy terms act in synergy. This appears clearly in the much larger formation energy difference between ZrS_2 1T′ and 1H/1H* ribbons in Fig. 3, compared to MoS_2, WS_2, or $MoSe_2$. Additionally, no similar mechanism of structural width-driven transition could exist in ribbons with nonpolar edges, such as armchair ribbons.

The critical width N_c at which the 1T′/1H transition takes place can be estimated from the equalization of the two formation energies (per edge formula units) of the 1H/1H* and 1T′ zigzag ribbons, each referred to its corresponding monolayer:

$$E_{\text{form}}'^{1T'}(N) = E_{\text{tot}}^{1T'}(N) - NE_\infty^{1T'},$$
$$E_{\text{form}}'^{1H/1H^*}(N) = E_{\text{tot}}^{1H/1H^*}(N) - NE_\infty^{1H}, \quad (2)$$

where $E_\infty^{1T'}$ and E_∞^{1H} stand for the infinite monolayer energies per formula units in the 1T′ and 1H phases, respectively, whose difference can be read in Table I. $E_{\text{form}}'^{1H/1H^*}$ and $E_{\text{form}}'^{1T'}$ no longer depend on N beyond $N = 2$–3 in the compounds under consideration. Their difference $E_{\text{form}}'^{1H} - E_{\text{form}}'^{1T'}$ amounts to 2.91, 3.56, and 2.68 eV per edge formula unit, in MoS_2, WS_2, and $MoSe_2$, respectively, whereas $E_{\text{form}}'^{1H^*} - E_{\text{form}}'^{1T'}$ equals 1.31, 1.64, and 1.29 eV in each case. Since the numbers of broken bonds at the 1T′ and 1H zigzag edges are equal, $E_{\text{form}}'^{1H} - E_{\text{form}}'^{1T'}$ principally represents the energy cost of edge polarity. It is related to charge compensation by band overlap, i.e., to the energy required to excite an electron from the top of the valence band to the bottom of the conduction band [17]. Indeed the values of $E_{\text{form}}'^{1H} - E_{\text{form}}'^{1T'}$ satisfactorily scale with the HOMO-LUMO gaps of the 1H monolayers: 1.56, 1.90, and 1.51 eV, respectively. The same holds for $E_{\text{form}}'^{1H^*} - E_{\text{form}}'^{1T'}$. N_c can then be expressed in the following way:

$$N_c^{1H/1H^*} = \frac{E_{\text{form}}'^{1H/1H^*} - E_{\text{form}}'^{1T'}}{E_\infty^{1T'} - E_\infty^{1H}}. \quad (3)$$

Despite their different edge composition and a very different stability, both 1H and 1H* ribbons display a similar stability crossover towards the 1T′ phase as a function of ribbon width. It is worth pointing out that the reported values of N_c are likely underestimated due to the well-known underestimation of GGA gaps, but this shortcoming is not expected to bias the predicted evolution in the series nor its relationship to polarity.

An interesting outcome of the structural change is the existence of a sound modification in the electronic properties of the nanoribbons at the 1T′/1H phase transition. This is due to the different electronic character of the MoS_2, WS_2, and $MoSe_2$ 1T′ and 1H infinite monolayers: metallic in the 1T′ phase; semiconducting in the 1H phase. As a consequence, accompanying the structural phase transition, the cores of the ribbons experience a metal to semiconducting transition at N_c, which is expected to drastically change their transport as well as optical properties.

VI. CONCLUSION

Relying on first-principles simulations, we have predicted the existence of a small width regime in several TMD zigzag ribbons of monolayer thickness. It is characterized by a dimerized 1T′ structure, at variance with the 1H structure characteristic of wider ribbons, infinite monolayers, and bulk materials. While the metastable 1T′ structural phase of the infinite MoS_2 monolayer has only been observed under very restricted synthesis conditions, in the present study we predict it to be the actual ground state of MoS_2, WS_2, and $MoSe_2$ monolayer-thick zigzag nanoribbons of small width. We assign this result to the competition between edge energy which favors the nonpolar 1T′ edges over the polar 1H edges, and energy of atoms in the ribbon center, which favors the 1H ground state of the infinite monolayers in these TMDs. At small width, due to the high value of the edge-to-bulk ratio, edge effects are dominant and drive the systems to the 1T′ ground state with no polarity and thus low edge energy. The mechanism is similar to the one predicted and confirmed in polar ultrathin films, such as MgO(111) or ZnO(0001), which display nonpolar (0001) surfaces of hexagonal BN structure at small thickness rather than polar (111) rocksalt surfaces or (0001) wurtzite ones. We have shown that the critical width at which the stability inversion takes place depends

on the cost of edge polarity, driven by the gap width in the 1H monolayer, and definitely falls into the observable range. A metal-to-semiconductor transition accompanies the 1T′/1H phase transition. At variance, ZrS_2 zigzag ribbons are predicted to display the 1T′ structure whatever their width, because this structure is favored by atoms both in the ribbon center and at its edges. In compounds of major technological importance, such structural and electronic flexibility associated with polarity effects opens the possibility for controlling the ribbon type during synthesis.

ACKNOWLEDGMENTS

F.G. and A.M.L. belong to the Institute of Nanoscience and Nanotechnology (INN) of the Atomic Energy Agency (CNEA), Argentina. They acknowledge financial support from ANPCyT (PICT-2011-1187 and PRH074) and CONICET (PIP00273). We gratefully acknowledge a generous allocation of computing time at IDRIS, under Project No. 100170 and support from the COST action CM1104 "Reducible oxide chemistry, structure and functions."

[1] Q. H. Wang, K. Kalantar-Zadeh, A. Kis, J. N. Coleman, and M. S. Strano, Nat. Nanotechnol. **7**, 699 (2012).
[2] A. B. Kaul, J. Mater. Res. **29**, 348 (2014).
[3] S. Helveg, J. V. Lauritsen, E. Lægsgaard, I. Stensgaard, J. K. Nørskov, B. S. Clausen, H. Topsøe, and F. Besenbacher, Phys. Rev. Lett. **84**, 951 (2000).
[4] J. Lauritsen, M. V. Bollinger, E. L. K. W. Jacobsen, J. K. Nørskov, B. S. Clausen, H.Topsøe, and F. Besenbacher, J. Catal. **221**, 510 (2004).
[5] H. Schweiger, P. Raybaud, G. Kresse, and H. Toulhoat, J. Catal. **207**, 76 (2002).
[6] R. Shidpour and M. Manteghian, Chem. Phys. **360**, 97 (2009).
[7] N. Peimyoo, J. Shang, C. Cong, X. Shen, X. Wu, E. K. L. Yeow, and T. Yu, ACS Nano **7**, 10985 (2013).
[8] M. V. Bollinger, J. V. Lauritsen, K. W. Jacobsen, J. K. Nørskov, S. Helveg, and F. Besenbacher, Phys. Rev. Lett. **87**, 196803 (2001).
[9] M. V. Bollinger, K. W. Jacobsen, and J. K. Nørskov, Phys. Rev. B. **67**, 085410 (2003).
[10] A. R. Botello-Mendez, F. López-Urías, M. Terrones, and H. Terrones, Nanotechnology **20**, 325703 (2009).
[11] C. Ataca, H. Sahin, E. Akturk, and S. Ciraci, J. Phys. Chem. C **115**, 3934 (2011).
[12] E. Erdogan, I. Popov, A. Enyashin, and G. Seifert, Eur. Phys. J. B **85**, 33 (2012).
[13] N. Huo, Y. Li, J. Kang, R. Li, Q. Xia, and J. Li, Appl. Phys. Lett. **104**, 202406 (2014).
[14] F. Ouyang, X. Ni, Z. Yang, Y. Chen, X. Zheng, and X. Xiong, J. Appl. Phys. **114**, 213701 (2013).
[15] F. Güller, A. M. Llois, J. Goniakowski, and C. Noguera, Phys. Rev. B **87**, 205423 (2013).
[16] J. Goniakowski, F. Finocchi, and C. Noguera, Rep. Prog. Phys **71**, 16501 (2008).
[17] C. Noguera and J. Goniakowski, Chem. Rev. **113**, 4073 (2013).
[18] J. Goniakowski, C. Noguera, and L. Giordano, Phys. Rev. Lett. **93**, 215702 (2004).
[19] F. Claeyssens, C. L. Freeman, N. L. Allan, Y. Sun, M. N. Ashfold, and J. H. Harding, J. Mater. Chem. **15**, 139 (2005).
[20] C. Tusche, H. L. Meyerheim, and J. Kirschner, Phys. Rev. Lett. **99**, 026102 (2007).
[21] C. L. Freeman, F. Claeyssens, N. L. Allan, and J. H. Harding, Phys. Rev. Lett. **96**, 066102 (2006).
[22] B. J. Morgan, Phys. Rev. B **80**, 174105 (2009).
[23] Y.-C. Lin, D. O. Dumcenco, Y.-S. Huang, and K. Suenaga, Nat. Nanotechnol. **9**, 391 (2014).
[24] D. Yang, S. J. Sandoval, W. M. R. Divigalpitiya, J. C. Irwin, and R. F. Frindt, Phys. Rev. B **43**, 12053 (1991).
[25] X. R. Qin, D. Yang, R. F. Frindt, and J. C. Irwin, Phys. Rev. B **44**, 3490 (1991).
[26] E. Prouzet, J. Heising, and M. G. Kanatzidis, Chem. Mater. **15**, 412 (2003).
[27] G. Eda, H. Yamaguchi, D. Voiry, T. Fujita, M. Chen, and M. Chhowalla, Nano Lett. **11**, 5111 (2011).
[28] G. Eda, T. Fujita, H. Yamaguchi, D. Voiry, M. Chen, and M. Chhowalla, ACS Nano **6**, 7311 (2012).
[29] T. Hu, R. Li, and J. Dong, J. Chem. Phys. **139**, 174702 (2013).
[30] M. Calandra, Phys. Rev. B **88**, 245428 (2013).
[31] G.Kresse and J. Furthmüller, Phys. Rev. B **54**, 11169 (1996).
[32] G. Kresse and D. Joubert, Phys. Rev. B **59**, 1758 (1999).
[33] J. P. Perdew and Y. Wang, Phys. Rev. B **45**, 13244 (1992).
[34] R. F. W. Bader, Chem. Rev. **91**, 893 (1991).
[35] W. Tang, E. Sanville, and G. Henkelman, J. Phys. Condens. Matter **21**, 084204 (2009).